mathematics

MDPI

Article

Vibrations of Nonlocal Polymer-GPL Plates at Nanoscale: Application of a Quasi-3D Plate Model

Yunhe Zou [1,2,*] and Yaser Kiani [3,*]

[1] School of Mechanical Engineering, Inner Mongolia University of Technology, Hohhot 010051, China
[2] Inner Mongolia Key Laboratory of Special Service Intelligent Robotics, Hohhot 010051, China
[3] Faculty of Engineering, Shahrekord Univeristy, Shahrekord P.O. Box 115, Iran
* Correspondence: zouyh@imut.edu.cn (Y.Z.); y.kiani@aut.ac.ir or y.kiani@sku.ac.ir (Y.K.)

Abstract: An analysis is performed in this research to obtain the natural frequencies of a graphene-platelet-reinforced composite plate at nanoscale. To this end, the nonlocal elasticity theory is applied. A composite laminated plate is considered where each layer is reinforced with GPLs. The amount of GPLs may be different between the layers, which results in functionally graded media. To establish the governing equations of the plate, a quasi-3D plate model is used, which takes the non-uniform shear strains as well as normal strain through the thickness into account. With the aid of the Hamilton principle, the governing equations of the plate are established. For the case of a plate that is simply supported all around, natural frequencies are obtained using the well-known Navier solution method. The results of this study are compared with the available data in the open literature, and, after that, novel numerical results are provided to explore the effects of different parameters. It is depicted that, with the introduction of GPLs in the matrix of the composite media, the natural frequencies of the plate enhance. Also, a proper graded pattern in GPL-reinforced composite plates, i.e., an FG-X pattern, results in the maximum frequencies of the plate. In addition, the introduced quasi-3D plate theory is accurate in the estimation of the natural frequencies of thick nanocomposite plates at nanoscale.

Keywords: graphene platelet; nonlocal theory; quasi-3D plate model; Navier method

MSC: 74K20; 74H45; 74E30; 74B05; 74G05

Citation: Zou, Y.; Kiani, Y. Vibrations of Nonlocal Polymer-GPL Plates at Nanoscale: Application of a Quasi-3D Plate Model. *Mathematics* **2023**, *11*, 4109. https://doi.org/10.3390/math11194109

Academic Editor: Dongfang Li

Received: 23 August 2023
Revised: 21 September 2023
Accepted: 27 September 2023
Published: 28 September 2023

1. Introduction

Technology's insatiable thirst to provide materials with greater and greater strength-to-weight ratios is what has drawn attention to GPL-reinforced composites. In recent years, graphene platelet has taken the place of its rival at the top of the table of optimal reinforcements due to its larger load-transfer surface and significant advantages in the nanocomposite manufacturing process compared to another pioneering reinforcement, e.g., carbon nanotube (CNT). For instance, Rafiei et al. [1], in their experimental work, highlighted that GPL-reinforced composites may exhibit 10 times the strength and also 1.3 times the Young's modulus when compared to CNT-reinforced composites. On the other hand, functionally graded materials (FGMs), owing to their controllability over mechanical properties in the required directions, are evaluated as the state-of-the-art materials. Today, the combination of two concepts of GPL-reinforced composite materials and functionally graded material, namely functionally graded graphene-reinforced composite (FG-GPLRC) materials, have unanimously been considered as one of the most promising and most interesting research topics [2].

On the basis of the first-order shear deformation theory, Song et al. [3] presented the free and forced vibration analysis on functionally graded GPL-reinforced plates. The vibration frequencies of FG-GPLRC plates were investigated by Guo et al. [4] by employing the element-free IMLS-Ritz method. Zhao et al. [5] proposed an FEM-based analysis around the

free vibration and bending behavior of composite trapezoidal plates made of GPLRC layers. The bending response of functionally graded reinforced graphene nanoplatelet (GNP) quadrilateral plates was obtained by Guo el al. [6] with the aid of the element-free IMLS-Ritz method. Gholami and Ansari [7] took the von Kármán-type nonlinearity into account to investigate the nonlinear stability and free vibration of FG-GPLRC plates subjected to compressive in-plane mechanical loads. Wu et al. [8] presented a numerical study on the parametric instability of FG-GPLRC plates under periodic uniaxial mechanical load and a uniform thermal load via the generalized quadrature method. Reddy et al. [9] used the finite element model on the basis of first-order shear deformation theory assumptions to probe the vibratory features of thin/moderately thick/thick composite plates made of GPL-reinforced plies. Gao et al. [10] estimated the effective elastic modulus of the GPL-reinforced composite media with the accordance of the assumption of closed-cell cellular solids under Gaussian random field scheme to obtain the vibration frequency of functionally graded GPL-reinforced porous plates. Yang et al. [11] employed the Chebyshev–Ritz solution method to derive buckling loads and natural frequencies of porous GPL-reinforced laminated plates modeled with FSDT assumptions. Functionally graded GPL-reinforced laminated composite plate that was undergoing in-plane excitations and electrical voltage was subjected to free vibration and nonlinear aeroelastic analysis by Lin et al. [12] in a high-order shear deformation model. Gholami and Ansari [13] developed a numerical analysis around the nonlinear vibration behavior of thick and moderately thick FG-GPLRC rectangular plates on the basis of assumptions of a higher-order shear deformation model. By employing Mindlin's plate model and the phase-field approach, Torabi and Ansari [14] studied the vibration behavior of graphene-platelet-reinforced multilayer composite plates with the consideration of stationary crack. Within a higher-order shear deformation model, the analysis of variance on the natural frequencies of composite plates made of GPL-reinforced plies was presented by Pashmforoush [15]. Ansari et al. [16] proposed a numerical approach on the basis of variational differential quadrature (VDQ) and the finite element method (FEM) to study the postbuckling response and free vibration of buckled FG-GPLRC plates in an HSDT model. Zhao et al. [17] adopted the small parameter perturbation method to obtain the free/forced vibration response of rotating FG-GPLRC plates under the action of rub-impact and thermal shock. Thai and Phung-Van [18] employed a moving Kriging (MK) using a naturally stabilized nodal integration (NSNI) within the framework of a higher-order shear deformation model to obtain the free vibration characteristics of functionally graded GPL-reinforced plates of complicated shapes. Exploiting a quasi-3D plate model, Jafari and Kiani [19] highlighted the free vibration characteristics of thick composite plates made of functionally graded GPL-reinforced materials. Shi et al. [20] performed static and free vibration investigation of functionally graded porous skew plates with GPL reinforcements, utilizing a three-dimensional elasticity model. Through a Ritz formulation, Kiani and Zur [21] planned a frequency analysis on functionally graded graphene-platelet-reinforced skew plates resting on point supports. Regarding the assumptions of the first-order shear deformation theory (FSDT) and the modified couple stress theory (MCST), Abbaspour et al. [22] formulated active control of vibration of GPL-reinforced composite micro-plates with piezoelectric face sheets.

Conducting experimental studies on nanoscale structures is not economically justified and is very difficult. Mathematical modeling is a way to overcome this issue. Molecular dynamics (MD) and continuum mechanics (CM) approaches are the most widely used types of mathematics-based modeling. Although MD modeling is much more accurate, its limitations, i.e., computationally expensive costs and time-consuming simulation, present it as a non-optimal choice for practical applications, and this is the point on which the reason and justification for more adoption of CM modeling, despite its lower accuracy, are based on.

When it comes to studying nanostructures, the limitation of classical CM models in considering size effects produces significant errors. For this reason, various size-dependent models have been released so far. Eringen's nonlocal theory [23] is one of the well-known

and popular continuum mechanics theories that has the ability to include nano-scale effects with appropriate accuracy. Employing Eringen's nonlocal theory can enable researchers to predict the static/dynamic behavior of a nanostructure without exploiting a large number of equations. By correlating nonlocal theory with different plate theories, such as the classical plate theory (CPT), first-order shear deformation theory (FSDT) [24], and higher-order shear deformation theory (HSDT) [25,26], various nonlocal models for nanoplate analyses have been extended.

For instance, in the framework of Kirchhoff and the Mindlin plate theories, behaviors of isotropic nanoplates are probed by Lu et al. [27] through a size-dependent nonlocal model. References [28–31] refer to more development of this model via analytical approaches. Karami et al. [32–34] investigated the dynamic behavior of functionally graded graphene-nanoplatelet-reinforced doubly curved polymer composite nanoshells based on a nonlocal model. Wave dispersion was also discussed in detail. Furthermore, Pradhan and Phadikar [35] dealt with free vibration analysis of nano-plates on the basis of a couple of classical plate theory (CLPT) and nonlocal FSDT models. This model was also employed in studies highlighted in [36,37]. Panyatong et al. [38] developed a second-order shear deformation model to perform an analytical study on the free vibration characteristics of the functionally graded (FG) nanoplates surrounded by an elastic medium based on Eringen's nonlocal elasticity. In the framework of a nonlocal four-variable plate model, Barati and Shahverdi [39] used the homotopy perturbation method to present new numerical solutions of nonlinear vibration of a porous nanoplate rested on a nonlinear elastic foundation. Further, Aghababaei and Reddy [40] obtained analytical solutions of free vibration of a simply supported nanoplate with the accordance of the assumptions of a nonlocal third-order shear deformation model. In this regard, based on a higher-order shear deformation theory of plates, Daneshmehr et al. [41] utilized the generalized differential quadrature method (GDQM) to calculate the free vibration frequencies of nanoplates, considering small scale effects with the aid of the nonlocal model. An isogeometric-based finite element method was implemented by Natarajan et al. [42] to compute the fundamental frequency of nanoplates made of functionally graded materials. Size dependency was considered via a nonlocal model. Cutolo et al. [43] formulated free vibrations and buckling of a functionally graded thick nanoplate placed on a Winkler–Pasternak foundation based on third-order shear deformation theory and nonlocal elasticity formulation. Based on the assumptions of simple inverse hyperbolic shear deformation theory and nonlocal elasticity theory, Pun-Van et al. [44] mathematically modeled the isogeometric approach on free vibrations of GPLRC. Xie et al. [45] proposed a novel nonlocal higher-order theory to obtain accurate vibration properties of 2D functionally graded nanoplates.

As the literature survey demonstrates, the vibrational behavior of functionally graded GPL-reinforced multilayer thick nanoplates through a nonlocal quasi-3D model has not been explored so far, and this is what motivated us to plan the current research. To perform a numerical study, effective mechanical properties of GPLRC layers are estimated based on a modified Halpin–Tsai micromechanical model and the rule of mixtures. In order to obtain the effects of non-uniform shear strains through the thickness, thickness stretching effects, and size-dependent effects, governing equations are derived via a nonlocal quasi-3D model and are solved with extending a Navier solution method. Comparative studies confirm the accuracy of the results and provide the credibility to perform parametric studies. The rest of the article is allocated to parametric studies around the effects of number of layers, nonlocal parameters, length-to-thickness ratio, GPL weight fraction, and distribution pattern of GPLs.

2. Problem Statement

In this section, the basics of the GPLRC nanoplate are provided. The methods of the evaluation of the material properties are provided, and, also, the functionally graded patterns of the GPLs are introduced.

Herein, an N_L-layer functionally graded graphene-reinforced nanoplate with a-length, b-width, and h-height is under free vibration study. To evaluate the deformations, a right-handed coordinate system that has its origin at the corner of the plate is located in the middle surface of the plate so that the axes x, y, and z are through the length, width, and thickness directions. Figure 1 provides the schematic of the plate.

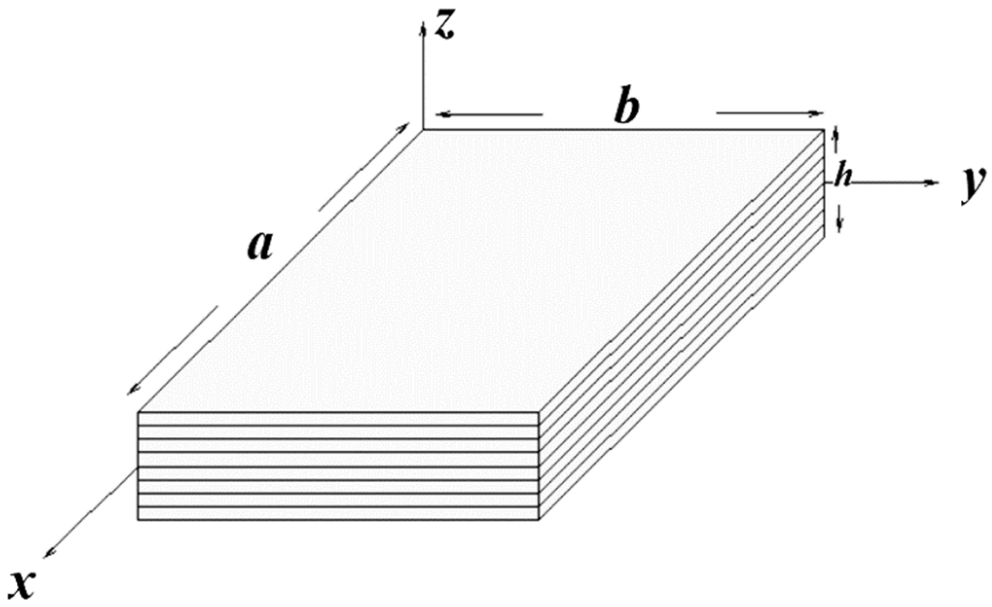

Figure 1. Configuration and coordinates of the FG-GPLRC nanoplate.

The volume fraction of GPLs through the k-th layer, which is highly dependent on the scattering patterns of GPL across the thickness direction of the nanoplate, plays a key role in estimating the mechanical properties of the k-th layer. The impacts of GPLs distribution pattern on the free vibration characteristics of multilayer FG-GPLRC nanoplate are evaluated by considering four patterns of GPLs distribution, which are achieved by functionally arranging the layers reinforced with different values of GPL's volume fraction. Figure 2 provides the patterns.

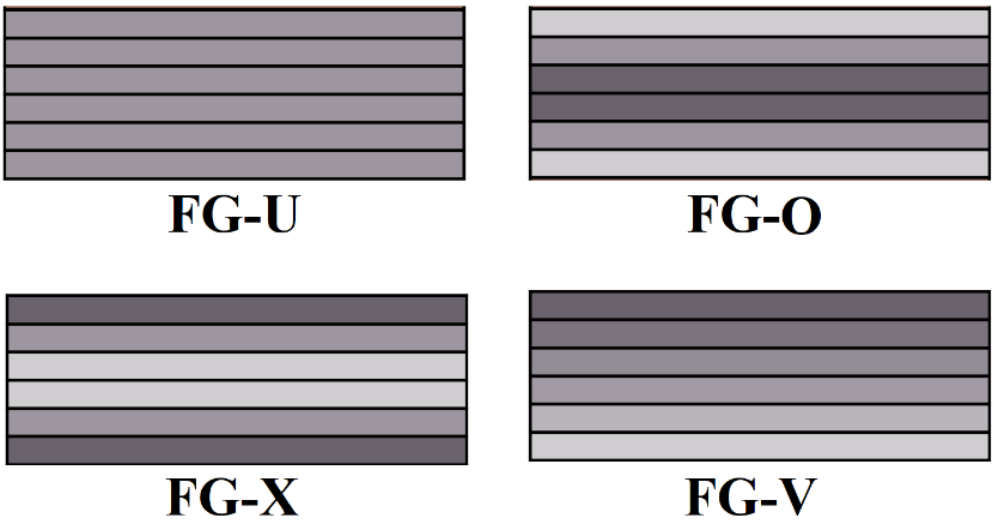

Figure 2. Dispersion patterns of GPLs.

Based on the first pattern, the volume fraction of GPLs is considered the same in all layers, besides in the cases of the non-uniform pattern; the highest volume fraction of GPLs

is allocated to the outer layers, the middle layer, and the upper layer, respectively, whose mathematical expressions in terms of the total volume fraction of GPLs across the plate, V^*_{GPL}, take the following form:

$$\begin{aligned} V^{(k)}_{GPL} &= V^*_{GPL} && \text{FG}-\text{U} \\ V^{(k)}_{GPL} &= 2V^*_{GPL}\tfrac{|2k-N_L-1|}{N_L} && \text{FG}-\text{X} \\ V^{(k)}_{GPL} &= 2V^*_{GPL}\left(1-\tfrac{|2k-N_L-1|}{N_L}\right) && \text{FG}-\text{O} \\ V^{(k)}_{GPL} &= V^*_{GPL}\tfrac{2k-1}{N_L} && \text{FG}-\text{V} \end{aligned} \tag{1}$$

For the k-th layer, which is reinforced with randomly oriented and uniformly dispersed GPLs, the effective Young's modulus based upon the modified Halpin–Tsai scheme can be read as follows [4]

$$E^{(k)} = \tfrac{1}{8}E_m\left(3\tfrac{1+\xi_L\eta_L V^{(k)}_{GPL}}{1-\eta_L V^{(k)}_{GPL}} + 5\tfrac{1+\xi_T\eta_T V^{(k)}_{GPL}}{1-\eta_T V^{(k)}_{GPL}}\right) \quad (k=1,2,\ldots,N_L) \tag{2}$$

where $V^{(k)}_{GPL}$ is the volume fraction of GPLs in k-th layer. Moreover, E_m stands for the Young's modulus of the polymer matrix and η_L and η_T are defined as

$$\eta_L = \frac{\frac{E_{GPL}}{E_m}-1}{\frac{E_{GPL}}{E_m}+\xi_L} \qquad \eta_T = \frac{\frac{E_{GPL}}{E_m}-1}{\frac{E_{GPL}}{E_m}+\xi_T} \tag{3}$$

E_{GPL} denotes the elasticity modulus of the GPLs, and the effects of the size and geometry of the nanoscale reinforcements are included in ξ_L and ξ_T according to the following relations

$$\xi_L = 2\frac{l_{GPL}}{h_{GPL}} \qquad \xi_T = 2\frac{w_{GPL}}{h_{GPL}} \tag{4}$$

In Equation (4), l_{GPL}, w_{GPL}, and h_{GPL} symbolize the average length, width, and thickness of the GPLs, respectively.

On the basis of rule of mixtures, the effective mass density $(\rho^{(k)})$ and Poisson's ratio $(\nu^{(k)})$ are acquired as

$$\begin{aligned} \nu^{(k)} &= \nu_m\left(1-V^{(k)}_{GPL}\right)+\nu_{GPL}V^{(k)}_{GPL} \\ \rho^{(k)} &= \rho_m\left(1-V^{(k)}_{GPL}\right)+\rho_{GPL}V^{(k)}_{GPL} \end{aligned} \tag{5}$$

It is worth highlighting that the parameters related to matrix and GPLs are separated by applying subscripts m and GPL.

3. Displacements and Strains

In this study, a quasi-3D plate model is utilized to investigate the free vibration of the arbitrary thick FG-GPLRC nanoplates. Adopting such a model provides the possibility to consider thickness stretching and also non-uniform transverse shear strain components as well as satisfying the condition of traction-free at bottom and top surfaces. Based upon this theory, displacement field may be written as [19]:

$$\mathbf{u} = \mathbf{u_0} + z\mathbf{u_1} + F(z)\boldsymbol{\Theta} \tag{6}$$

With the following definitions:

$$\mathbf{u} = \begin{Bmatrix} u \\ v \\ w \end{Bmatrix}, \mathbf{u_0} = \begin{Bmatrix} u_0 \\ v_0 \\ w_0 \end{Bmatrix}, \mathbf{u_1} = -\begin{Bmatrix} w_{0,x} \\ w_{0,y} \\ 0 \end{Bmatrix}, F(z) = \begin{bmatrix} f(z) & 0 & 0 \\ 0 & f(z) & 0 \\ 0 & 0 & f'(z) \end{bmatrix}, \boldsymbol{\Theta} = \begin{Bmatrix} \theta_x \\ \theta_y \\ \theta_z \end{Bmatrix} \tag{7}$$

where $\mathbf{u}$ is displacement vector of a material point located at (x, y, z), $\mathbf{u_0}$ is the displacement of a material point located at mid-plane, and $\mathbf{\Theta}$ is rotation vector. Moreover, based on Reddy third-order plate theory (TPT), $f(z) = z(1 - \frac{4z^2}{3h^3})$

In Equation (7), differentiation with respect to a parameter is symbolized with $()_{,}$.

The nonzero strain components in terms of displacement components can be evaluated as follows:

$$\begin{aligned} \{\varepsilon_{xx}, \varepsilon_{yy}, \varepsilon_{xy}\}^T &= \boldsymbol{\varepsilon^m} - z\boldsymbol{\kappa^m} + f(z)\boldsymbol{\kappa^\theta} \\ \{\varepsilon_{xz}, \varepsilon_{yz}\}^T &= f_{,z}\boldsymbol{\kappa^s} \\ \varepsilon_{zz} &= f_{,zz}\theta_z \end{aligned} \tag{8}$$

In which

$$\begin{aligned} \boldsymbol{\varepsilon^m} &= \{u_{0,x}, v_{0,y}, (u_{0,y} + v_{0,x})/2\}^T \\ \boldsymbol{\kappa^m} &= \{w_{0,xx}, w_{0,yy}, w_{0,xy}\}^T \\ \boldsymbol{\kappa^\theta} &= \{\theta_{x,x}, \theta_{y,y}, (\theta_{x,y} + \theta_{y,x})/2\}^T \\ \boldsymbol{\kappa^s} &= \{\theta_{z,x} + \theta_x, \theta_{z,y} + \theta_y\}^T \end{aligned} \tag{9}$$

where, in Equation (9), $\boldsymbol{\varepsilon^m}$ indicates the mid-surface strains and $\boldsymbol{\kappa^m}$ stands for the curvatures. Also, higher-order curvatures are denoted by $\boldsymbol{\kappa^\theta}$ and refined shear strains are $\boldsymbol{\kappa^s}$.

4. Local Constitutive Relations

Considering 3D case of stress, the 3D constitutive equations of the k-th layer can be written as

$$\boldsymbol{\sigma}^{(k)} = \mathbf{C}^{(k)}\boldsymbol{\varepsilon} \tag{10}$$

According to the mathematical expression presented in Equation (5), the stress vector, $\boldsymbol{\sigma}^{(k)} = \left\{{\sigma_{xx}}^{(k)}, {\sigma_{yy}}^{(k)}, {\sigma_{zz}}^{(k)}, {\sigma_{xz}}^{(k)}, {\sigma_{yz}}^{(k)}, {\sigma_{xy}}^{(k)}\right\}^T$ is achieved by the strain vector, $\boldsymbol{\varepsilon} = \{\varepsilon_{xx}, \varepsilon_{yy}, \varepsilon_{zz}, 2\varepsilon_{xz}, 2\varepsilon_{yz}, 2\varepsilon_{xy}\}^T$ left-multiplied by the stiffness matrix, $\mathbf{C}^{(k)}$, which has the following definition:

$$\mathbf{C}^{(k)} = \begin{bmatrix} Q_{11} & Q_{12} & Q_{13} & 0 & 0 & 0 \\ Q_{21} & Q_{22} & Q_{23} & 0 & 0 & 0 \\ Q_{31} & Q_{32} & Q_{33} & 0 & 0 & 0 \\ 0 & 0 & 0 & Q_{44} & 0 & 0 \\ 0 & 0 & 0 & 0 & Q_{55} & 0 \\ 0 & 0 & 0 & 0 & 0 & Q_{66} \end{bmatrix} \tag{11}$$

${Q_{ij}}'s (i = 1, 2, \ldots, 6$ and $j = 1, 2, \ldots, 6)$ are the elastic components, of which the nonzero ones are obtained according to the following relations:

$$\begin{aligned} Q_{11} = Q_{22} = Q_{33} &= \frac{E^{(k)}\left(1-v^{(k)}\right)}{\left(1+v^{(k)}\right)\left(1-2v^{(k)}\right)} \\ Q_{12} = Q_{21} = Q_{13} = Q_{31} = Q_{23} = Q_{32} &= \frac{E^{(k)}v^{(k)}}{\left(1+v^{(k)}\right)\left(1-2v^{(k)}\right)} \\ Q_{44} = Q_{55} = Q_{66} &= \frac{E^{(k)}}{2\left(1+v^{(k)}\right)} \end{aligned} \tag{12}$$

5. Nonlocal Model

Herein, to perform a more accurate numerical investigation on nanoscale structures, the nano-scale effects are considered by adopting the nonlocal elasticity theory first proposed by Eringen [23]. The concept behind this theory is that the stress at a point in an elastic continuum has dependency on the strains at points located throughout the continuum, unlike classical theories in which the stress evolution at one point is assumed to be unrelated to the strains at other points. Eringen [23] developed a mathematical relation

between local stress tensor σ_{ij} and nonlocal stress tensor t_{ij} by introducing the nonlocal parameter μ, whose simplified differential form can be approximated as follows:

$$t_{ij} = \left(1 - \mu\nabla^2\right)\sigma_{ij} \tag{13}$$

where $\nabla^2 = \left(\frac{\partial}{\partial x^2} + \frac{\partial}{\partial y^2}\right)$ signifies to the second Laplace operator. Furthermore, the nonlocal parameter is defined as $\mu = (e_0 a_{NL})^2$, in which e_0 is a material constant and a_{NL} is an internal characteristic length, which are material dependent parameters that should be determined through experimental research or simulation of atomistic dynamics. The nonlocal stress–strain relation for the k-th layer of the FG-GPLRC nanoplate is established in following form:

$$\mathbf{t}^{(k)} = \left(1 - \mu\nabla^2\right)\boldsymbol{\sigma}^{(k)} = \mathbf{C}^{(k)}\boldsymbol{\varepsilon} \tag{14}$$

6. Governing Equations of Motion

The governing equations of motion are derived with the aid of the variation form of Hamilton's principle:

$$\int_0^t (\delta U - \delta K)dt = 0 \tag{15}$$

The components of the Hamilton principle, the variation of strain energy (δU) and kinetic energy (δK), are calculated through the following expressions [19]:

$$\begin{aligned}
\delta U &= \int_0^b \int_0^a \sum_{k=1}^{N_L} \int_{h_{k-1}}^{h_k} \left(\sigma_{xx}{}^{(k)}\delta\varepsilon_{xx} + \sigma_{yy}{}^{(k)}\delta\varepsilon_{yy} + \sigma_{zz}{}^{(k)}\delta\varepsilon_{zz} + 2\sigma_{xy}{}^{(k)}\varepsilon_{xy} + 2\sigma_{xz}{}^{(k)}\delta\varepsilon_{xz} + 2\sigma_{yz}{}^{(k)}\delta\varepsilon_{yz}\right)dzdxdy \\
\delta K &= \int_0^b \int_0^a \sum_{k=1}^{N_L} \int_{h_{k-1}}^{h_k} \left(\rho^{(k)}\left\{\dot{u}\delta\dot{u} + \dot{v}\delta\dot{v} + \dot{w}\delta\dot{w}\right\}\right)dzdxdy
\end{aligned} \tag{16}$$

By substituting Equations (7) and (10) into Equation (16), introducing Equation (16) into Equation (15), applying the nonlocal relations of Equation (14), and performing the integrations over the thickness domain and also relieving the virtual displacements by applying the Green–Gauss theorem, the motion equations of the FG-GPLRC nanoplates are obtained from Hamilton's principle expressed in Equation (17)

$$\begin{aligned}
\delta u_0 \quad &: \quad N_{xx,x} + N_{xy,y} = I_1\ddot{u}_0 - I_2\ddot{w}_{0,x} + I_4\ddot{\theta}_x - \nabla^2\left(J_1\ddot{u}_0 - J_2\ddot{w}_{0,x} + J_4\ddot{\theta}_x\right) \\
\delta v_0 \quad &: \quad N_{yy,y} + N_{xy,x} = I_1\ddot{v}_0 - I_2\ddot{w}_{0,y} + I_4\ddot{\theta}_y - \nabla^2\left(J_1\ddot{v}_0 - J_2\ddot{w}_{0,y} + J_4\ddot{\theta}_y\right) \\
\delta w_0 \quad &: \quad M_{xx,xx} + M_{yy,yy} + 2M_{xy,xy} = I_1\ddot{w}_0 + I_2\left(\ddot{u}_{0,x} + \ddot{v}_{0,y}\right) - \\
&I_3\left(\ddot{w}_{0,xx} + \ddot{w}_{0,yy}\right) + I_5\left(\ddot{\theta}_{x,x} + \ddot{\theta}_{y,y}\right) + I_7\ddot{\theta}_z - \nabla^2\left(J_1\ddot{w}_0 + J_2\left(\ddot{u}_{0,x} + \ddot{v}_{0,y}\right) - \right. \\
&\left. J_3\left(\ddot{w}_{0,xx} + \ddot{w}_{0,yy}\right) + J_5\left(\ddot{\theta}_{x,x} + \ddot{\theta}_{y,y}\right) + J_7\ddot{\theta}_z\right) \\
\delta\theta_x \quad &: \quad -R_{xz} + P_{xx,x} + P_{xy,y} = I_4\ddot{u}_0 - I_5\ddot{w}_{0,x} + I_6\ddot{\theta}_x - \nabla^2\left(J_4\ddot{u}_0 - J_5\ddot{w}_{0,x} + J_6\ddot{\theta}_x\right) \\
\delta\theta_y \quad &: \quad -R_{yz} + P_{xy,y} + P_{yy,y} = I_4\ddot{v}_0 - I_5\ddot{w}_{0,y} + I_6\ddot{\theta}_y - \nabla^2\left(J_4\ddot{v}_0 - J_5\ddot{w}_{0,y} + J_6\ddot{\theta}_y\right) \\
\delta\theta_z \quad &: \quad -S_{zz} + R_{xz,x} + R_{yz,y} = I_7\ddot{w}_0 - I_8\ddot{\theta}_z - \nabla^2\left(J_7\ddot{w}_0 - J_8\ddot{\theta}_z\right)
\end{aligned} \tag{17}$$

By performing integration over the thickness domain, the classical and higher-order stress resultants and local and nonlocal inertia parameters are determined with the following relations:

$$
\begin{Bmatrix} N_{xx} \\ N_{yy} \\ N_{xy} \end{Bmatrix} = \begin{bmatrix} A_{11} & A_{12} & 0 \\ A_{21} & A_{22} & 0 \\ 0 & 0 & A_{66} \end{bmatrix} \begin{Bmatrix} u_{0,x} \\ v_{0,y} \\ (u_{0,y} + v_{0,x}) \end{Bmatrix} + \begin{bmatrix} B_{11} & B_{12} & 0 \\ B_{21} & B_{22} & 0 \\ 0 & 0 & B_{66} \end{bmatrix} \begin{Bmatrix} w_{0,xx} \\ w_{0,yy} \\ 2w_{0,xy} \end{Bmatrix}
$$
$$
+ \begin{bmatrix} C_{11} & C_{12} & 0 \\ C_{21} & C_{22} & 0 \\ 0 & 0 & C_{66} \end{bmatrix} \begin{Bmatrix} \theta_{x,x} \\ \theta_{y,y} \\ (\theta_{x,y} + \theta_{y,x}) \end{Bmatrix} + \begin{bmatrix} 0 & 0 & D_{13} \\ 0 & 0 & D_{23} \\ 0 & 0 & 0 \end{bmatrix} \begin{Bmatrix} \theta_z \\ \theta_z \\ 0 \end{Bmatrix}
$$
$$
\begin{Bmatrix} M_{xx} \\ M_{yy} \\ M_{xy} \end{Bmatrix} = \begin{bmatrix} B_{11} & B_{12} & 0 \\ B_{21} & B_{22} & 0 \\ 0 & 0 & B_{66} \end{bmatrix} \begin{Bmatrix} u_{0,x} \\ v_{0,y} \\ (u_{0,y} + v_{0,x}) \end{Bmatrix} + \begin{bmatrix} E_{11} & E_{12} & 0 \\ E_{21} & E_{22} & 0 \\ 0 & 0 & E_{66} \end{bmatrix} \begin{Bmatrix} w_{0,xx} \\ w_{0,yy} \\ 2w_{0,xy} \end{Bmatrix}
$$
$$
+ \begin{bmatrix} F_{11} & F_{12} & 0 \\ F_{21} & F_{22} & 0 \\ 0 & 0 & F_{66} \end{bmatrix} \begin{Bmatrix} \theta_{x,x} \\ \theta_{y,y} \\ (\theta_{x,y} + \theta_{y,x}) \end{Bmatrix} + \begin{bmatrix} 0 & 0 & G_{13} \\ 0 & 0 & G_{23} \\ 0 & 0 & 0 \end{bmatrix} \begin{Bmatrix} \theta_z \\ \theta_z \\ 0 \end{Bmatrix}
$$
$$
\begin{Bmatrix} P_{xx} \\ P_{yy} \\ P_{xy} \end{Bmatrix} = \begin{bmatrix} C_{11} & C_{12} & 0 \\ C_{21} & C_{22} & 0 \\ 0 & 0 & C_{66} \end{bmatrix} \begin{Bmatrix} u_{0,x} \\ v_{0,y} \\ (u_{0,y} + v_{0,x}) \end{Bmatrix} + \begin{bmatrix} F_{11} & F_{12} & 0 \\ F_{21} & F_{22} & 0 \\ 0 & 0 & F_{66} \end{bmatrix} \begin{Bmatrix} w_{0,xx} \\ w_{0,yy} \\ w_{0,xy} \end{Bmatrix}
$$
$$
+ \begin{bmatrix} H_{11} & H_{12} & 0 \\ H_{21} & H_{22} & 0 \\ 0 & 0 & H_{66} \end{bmatrix} \begin{Bmatrix} \theta_{x,x} \\ \theta_{y,y} \\ (\theta_{x,y} + \theta_{y,x}) \end{Bmatrix} + \begin{bmatrix} 0 & 0 & J_{13} \\ 0 & 0 & J_{23} \\ 0 & 0 & 0 \end{bmatrix} \begin{Bmatrix} \theta_z \\ \theta_z \\ 0 \end{Bmatrix} \tag{18}
$$
$$
\begin{Bmatrix} R_{xz} \\ R_{yx} \end{Bmatrix} = \begin{bmatrix} L_{44} & 0 \\ 0 & L_{55} \end{bmatrix} \begin{Bmatrix} \theta_x + \theta_{z,x} \\ \theta_y + \theta_{z,y} \end{Bmatrix}
$$
$$
S_{zz} = D_{13}u_{0,x} + D_{23}v_{0,y} - G_{13}w_{0,xx} - G_{23}w_{0,yy} + J_{13}\theta_{x,x} + J_{23}\theta_{y,y} + P_{33}\theta_z
$$
$$
(I_1, I_2, I_3, I_4, I_5, I_6, I_7, I_8) = \sum_{1}^{N_L} \int_{h_{k-1}}^{h_k} \rho^{(k)} \left(1, z, z^2, f, zf, f, f_{,z}, {f_{,z}}^2\right) dz
$$
$$
J_i = \mu I_i
$$

In Equation (18), $A_{ij}, B_{ij}, C_{ij}, D_{ij}, E_{ij}, F_{ij}, G_{ij}, H_{ij}, J_{ij}, L_{ij}$, and P_{ij} are stiffness components and are calculated as

$$
\begin{gathered}
(A_{ij}, B_{ij}, C_{ij}, D_{ij}, E_{ij}, F_{ij}, G_{ij}, H_{ij}, J_{ij}, L_{ij}, P_{ij}) = \\
\sum_{1}^{N_L} \int_{h_{k-1}}^{h_k} Q_{ij}^{(k)} \left(1, z, f, f_{,zz}, z^2, zf, zf_{,zz}, f^2, ff_{,zz}, {f_{,z}}^2, {f_{,zz}}^2\right) dz
\end{gathered} \tag{19}
$$

7. Analytical Solution

In the current study, the motion equations of an FG-GPLRC nanoplate subjected to simply supported at all edges are solved exploiting Navier's solution technique. Aiming to implement this technique, compatible with the simply supported boundary conditions and derived governing equations, the unknown displacement functions are expanded as the following formula:

$$
\begin{aligned}
u_0(x,y,t) &= \sum_{n=1}^{\infty} \sum_{m=1}^{\infty} U_{mn} e^{i\omega t} \cos(\alpha x) \sin(\beta y) \\
v_0(x,y,t) &= \sum_{n=1}^{\infty} \sum_{m=1}^{\infty} V_{mn} e^{i\omega t} \sin(\alpha x) \cos(\beta y) \\
w_0(x,y,t) &= \sum_{n=1}^{\infty} \sum_{m=1}^{\infty} W_{mn} e^{i\omega t} \sin(\alpha x) \sin(\beta y) \\
\theta_x(x,y,t) &= \sum_{n=1}^{\infty} \sum_{m=1}^{\infty} X_{mn} e^{i\omega t} \cos(\alpha x) \sin(\beta y) \\
\theta_y(x,y,t) &= \sum_{n=1}^{\infty} \sum_{m=1}^{\infty} Y_{mn} e^{i\omega t} \sin(\alpha x) \cos(\beta y) \\
\theta_z(x,y,t) &= \sum_{n=1}^{\infty} \sum_{m=1}^{\infty} Z_{mn} e^{i\omega t} \sin(\alpha x) \sin(\beta y)
\end{aligned} \tag{20}
$$

In above, $\alpha = m\pi/a$ and $\beta = n\pi/b$ and ω signify to the frequency of the FG-GPLRC nanoplate, which endures m and n as half waves through the length and width of it. Moreover, $U_{mn}, V_{mn}, W_{mn}, X_{mn}, Y_{mn}$, and Z_{mn} are the unknown coefficients that should to be determined.

Applying the above-stated expansions to the governing equations, one can obtain

$$\left(\mathbf{K}-\omega^2\mathbf{M}\right)\left\{U_{mn} \quad V_{mn} \quad W_{mn} \quad X_{mn} \quad Y_{mn} \quad Z_{mn}\right\}^T=0 \tag{21}$$

where stiffness and inertia matrices are symbolized with **K** and **M**, respectively, and have the following nonzero elements:

$$\begin{aligned}
&\mathbf{K}_{11}=A_{11}\alpha^2+A_{66}\beta^2;\\
&\mathbf{K}_{12}=(A_{12}+A_{66})\alpha\beta;\\
&\mathbf{K}_{13}=-[B_{11}\alpha^3+(B_{12}+2B_{66})\alpha\beta^2]\\
&\mathbf{K}_{14}=C_{11}\alpha^2+C_{66}\beta^2;\\
&\mathbf{K}_{15}=(C_{12}+C_{66})\alpha\beta;\\
&\mathbf{K}_{16}=-D_{13}\alpha\\
&\mathbf{K}_{22}=A_{66}\alpha^2+A_{22}\beta^2;\\
&\mathbf{K}_{23}=-[B_{22}\beta^3+(B_{12}+2B_{66})\beta\alpha^2];\\
&\mathbf{K}_{24}=(C_{12}+C_{66})\alpha\beta;\\
&\mathbf{K}_{25}=C_{66}\alpha^2+C_{22}\beta^2;\\
&\mathbf{K}_{26}=-D_{23}\beta;\\
&\mathbf{K}_{33}=E_{11}\alpha^4+E_{22}\beta^4+(2E_{12}+4E_{66})\alpha^2\beta^2;\\
&\mathbf{K}_{34}=-[F_{11}\alpha^3+(F_{12}+2F_{66})\alpha\beta^2];\\
&\mathbf{K}_{35}=-[F_{22}\beta^3+(F_{12}+2F_{66})\beta\alpha^2];\\
&\mathbf{K}_{36}=G_{13}\alpha^2+G_{23}\beta^2;\\
&\mathbf{K}_{44}=H_{11}\alpha^2+H_{66}\beta^2+L_{55};\\
&\mathbf{K}_{45}=(H_{12}+H_{66})\alpha\beta;\\
&\mathbf{K}_{46}=(L_{55}-J_{13})\alpha;\\
&\mathbf{K}_{55}=H_{66}\alpha^2+H_{22}\beta^2+L_{44};\\
&\mathbf{K}_{56}=(L_{44}-J_{23})\beta;\\
&\mathbf{K}_{66}=L_{55}\alpha^2+L_{44}\beta^2+P_{33}\\
&\mathbf{M}_{11}=I_1+J_1(\alpha^2+\beta^2);\\
&\mathbf{M}_{13}=-\alpha(I_2+J_2(\alpha^2+\beta^2));\\
&\mathbf{M}_{14}=I_4+J_4(\alpha^2+\beta^2);\\
&\mathbf{M}_{22}=I_1+J_1(\alpha^2+\beta^2);\\
&\mathbf{M}_{23}=-\beta(I_2+J_2(\alpha^2+\beta^2));\\
&\mathbf{M}_{25}=I_4+J_4(\alpha^2+\beta^2);\\
&\mathbf{M}_{33}=I_1+J_1(\alpha^2+\beta^2)+(\alpha^2+\beta^2)(I_3+J_3(\alpha^2+\beta^2));\\
&\mathbf{M}_{34}=-\alpha(I_5+J_5(\alpha^2+\beta^2));\\
&\mathbf{M}_{35}=-\beta(I_5+J_5(\alpha^2+\beta^2));\\
&\mathbf{M}_{36}=I_7+J_7(\alpha^2+\beta^2);\\
&\mathbf{M}_{44}=I_6+J_6(\alpha^2+\beta^2);\\
&\mathbf{M}_{55}=I_6+J_6(\alpha^2+\beta^2);\\
&\mathbf{M}_{65}=I_7+J_7(\alpha^2+\beta^2);\\
&\mathbf{M}_{66}=I_8+J_8(\alpha^2+\beta^2);
\end{aligned} \tag{22}$$

Finally, non-trivial solution of Equation (21) will be the frequencies, and, based upon them, the responding mode shapes are achieved.

8. Results and Discussion

Herein, based upon the proposed nonlocal quasi-3D model and developed solution method, the natural frequencies of FG-GPLRC nonoplates with simply supported edges

are studied. It is assumed that the graphene platelets with a length of 2.5 nm, a width of 1.5 nm, a thickness of 0.3 nm, and with the mechanical properties provided in Table 1 reinforced the polymer nanoplate. The mechanical properties of the polymer matrix can also be found in Table 1.

Table 1. Mechanical properties of the materials.

Property Name	Epoxy	GPLs
Modulus of elasticity (E) [GPa]	3	1010
Density (ρ) [kg/m^3]	1200	1062.5
Poisson's ratio (ν)	0.34	0.186

This section is divided into two subsections: the first subsection is devoted to validation via comparative studies, and the parametric studies are provided in the next one.

8.1. Comparison Studies

As the first comparative case, consider a simply supported homogeneous square nanoplate with the Poisson's ratio $\nu = 0.3$. To check the accuracy and reliability of the suggested plate model, the fundamental frequency parameter $\left(\Omega^* = \omega h\sqrt{\rho/G}\right)$ values for various nonlocal parameters and various length-to-thickness ratios obtained using the two-variable plate theory [46], four-variable 2D plate model [47], and four-variable 3D plate model [47] are tabulated in Table 2 and are compared with the results of the present research. It can be observed that the present results are in good agreement with the published ones obtained through the other higher-order plate theories.

Table 2. Comparison of fundamental frequency Ω^* of a homogeneous square nanoplate.

a/h	μ/a^2	Two-Variable Model	Four-Variable 2D Model	Four-Variable 3D Model	Present
10	0	0.093029	0.093031	0.093228	0.093151
	0.01	0.085016	0.085017	0.085197	0.085127
	0.02	0.078771	0.078772	0.078939	0.078874
	0.03	0.073726	0.073728	0.073884	0.073823
20	0	0.023864	0.023864	0.023895	0.023872
	0.01	0.021808	0.021808	0.021837	0.021816
	0.02	0.020206	0.020206	0.020233	0.020213
	0.03	0.018912	0.018912	0.018937	0.018919

In the next validation study, which is presented in Table 3, the first non-dimensional natural frequency $\left(\Omega = \omega h\sqrt{\rho_m/E_m}\right)$ of a square 10-layer FG-GPLRC nanoplate reinforced with 1 percent by weight of GPLs for different values of length-to-thickness ratios, nonlocal parameters, and distribution patterns of GPLs is provided and compared with that reported by Phung-Van et al. [44]. It is easy to see that an excellent agreement exists between the results of the present research and that obtained by the nonlocal isogeometric model proposed by Phung-Van et al. [44].

8.2. Parametric Studies

After gaining confidence in the validity of the results, which was achieved with the aid of comparative studies in the previous subsection, in this subsection, novel data are provided to perform parametric studies around the effects of number of layers, nonlocal parameter, thickness ratio, and weight fraction of GPL, considering four types of GPL distribution patterns. Hereafter, the material properties of the constituents are as-

sumed in accordance with those provided in Table 1 and dimensionless nonlocal parameter and dimensionless frequency are used with the following definitions:

$$\begin{array}{l} \Omega = \omega h \sqrt{\rho_m / E_m} \\ \lambda = \mu / a^2 \end{array} \quad (23)$$

Firstly, the first six frequency parameters and the associated mode numbers of the square FG-GPLRC nanoplates reinforced with 1 percent by weight of GPLs are provided in Table 4. In addition, to better grasp the variation in fundamental frequency as a function of number of layers, Figure 3 is provided. Square platforms with $a/h = 5$ are assumed, and the non-dimensional nonlocal parameter is set equal to 0.05. It is worth mentioning, according to the symmetry of the geometry and the boundary conditions, that it is obvious to obtain the repetitive frequencies, but filling the cells of Table 4 with repeated frequency has been avoided. It can be seen in the provided data in the rows and columns of Table 4 that the number of layers and distribution patterns of GPLs have significant effects on the frequencies of the nanoplates. Except for the U-GPLRC nanoplate, in which, due to the same properties of individual layers, increasing the number of layers does not affect the frequency of the nanoplate, increasing the number of layers leads to a variation in the frequencies of the nanoplates, which causes an increasing trend in the X-GPLRC nanoplate and a decreasing trend in the V- and O-GPLRC nanoplates. Moreover, the effects of this increase on the higher frequencies of the nanoplate are evaluated stronger than the lower frequencies. It should be noted that the highest rate of change is observed in the X model, and the lowest in the V model. Considering that, with models with more than ten layers, natural frequency changes become very slow, as an important inference from this observation, a ten-layer model can be employed as a promising optimal candidate instead of a single-layer plate with continuous variation in material properties. A similar conclusion is reported by [48,49].

Table 3. Comparison of fundamental frequency parameter Ω in GPLRC plate with $W_{GPL} = 1\%$.

a/h	Pattern	$\mu/a^2 = 0$		$\mu/a^2 = 0.01$		$\mu/a^2 = 0.03$		$\mu/a^2 = 0.05$	
		Present	**[44]**	**Present**	**[44]**	**Present**	**[44]**	**Present**	**[44]**
5	Pure	0.2143	0.2132	0.1959	0.1948	0.1698	0.1690	0.1520	0.1513
	UD	0.2296	0.2285	0.2099	0.2088	0.1820	0.1811	0.1629	0.1621
	FG-X	0.2345	0.2326	0.2143	0.2126	0.1858	0.1843	0.1663	0.1650
	FG-O	0.2244	0.2241	0.2051	0.2048	0.1779	0.1776	0.1592	0.1590
	FG-V	0.2293	0.2281	0.2096	0.2085	0.1817	0.1808	0.1627	0.1618
10	Pure	0.0585	0.0584	0.0535	0.0534	0.0464	0.0463	0.0415	0.0415
	UD	0.0627	0.0626	0.0573	0.0572	0.0497	0.0496	0.0445	0.0444
	FG-X	0.0644	0.0641	0.0589	0.0585	0.0511	0.0508	0.0457	0.0454
	FG-O	0.0609	0.0611	0.0557	0.0559	0.0483	0.0484	0.0432	0.0434
	FG-V	0.0626	0.0625	0.0572	0.0571	0.0496	0.0495	0.0444	0.0443
50	Pure	0.0024	0.0024	0.0022	0.0022	0.0019	0.0019	0.0017	0.0017
	UD	0.0026	0.0026	0.0024	0.0024	0.0021	0.0021	0.0018	0.0019
	FG-X	0.0027	0.0027	0.0024	0.0024	0.0021	0.0021	0.0019	0.0019
	FG-O	0.0025	0.0025	0.0023	0.0023	0.0020	0.0020	0.0018	0.0018
	FG-V	0.0026	0.0026	0.0024	0.0024	0.0021	0.0021	0.0018	0.0019

Table 4. First five parameters Ω of an FG-GPLRC square nanoplate for various values of number of layers with $\frac{a}{h} = 5$, $W_{GPL} = 1\%$, and $\lambda = 0.05$.

Distribution Pattern	N_L	Ω_1	Ω_2	Ω_3	Ω_4	Ω_5
FG-U	4	0.16290(1,1)	0.26997(2,1)	0.32713(2,2)	0.35315(3,1)	0.38218(3,2)
	6	0.16290(1,1)	0.26997(2,1)	0.32713(2,2)	0.35315(1,3)	0.38218(2,3)
	8	0.16290(1,1)	0.26997(2,1)	0.32713(2,2)	0.35315(1,3)	0.38218(2,3)
	10	0.16290(1,1)	0.26997(1,2)	0.32713(2,2)	0.35315(3,1)	0.38218(2,3)
	12	0.16290(1,1)	0.26997(2,1)	0.32713(2,2)	0.35315(3,1)	0.38218(3,2)
	14	0.16290(1,1)	0.26997(1,2)	0.32713(2,2)	0.35315(3,1)	0.38218(3,2)
FG-X	4	0.16557(1,1)	0.27267(2,1)	0.32912(2,2)	0.35462(1,3)	0.38291(3,2)
	6	0.16608(1,1)	0.27323(2,1)	0.32960(2,2)	0.35503(1,3)	0.38323(2,3)
	8	0.16626(1,1)	0.27343(2,1)	0.32977(2,2)	0.35518(1,3)	0.38336(3,2)
	10	0.16634(1,1)	0.27353(2,1)	0.32986(2,2)	0.35526(1,3)	0.38342(2,3)
	12	0.16639(1,1)	0.27358(1,2)	0.32990(2,2)	0.35530(3,1)	0.38345(2,3)
	14	0.16642(1,1)	0.27361(2,1)	0.32993(2,2)	0.35533(1,3)	0.38347(3,2)
FG-O	4	0.16008(1,1)	0.26690(2,1)	0.32464(2,2)	0.35112(1,3)	0.38083(3,2)
	6	0.15950(1,1)	0.26619(1,2)	0.32397(2,2)	0.35049(1,3)	0.38027(2,3)
	8	0.15930(1,1)	0.26593(2,1)	0.32371(2,2)	0.35025(3,1)	0.38005(3,2)
	10	0.15921(1,1)	0.26581(2,1)	0.32360(2,2)	0.35014(3,1)	0.37995(3,2)
	12	0.15915(1,1)	0.26575(2,1)	0.32353(2,2)	0.35008(1,3)	0.37989(3,2)
	14	0.15912(1,1)	0.26571(1,2)	0.32349(2,2)	0.35004(3,1)	0.37985(3,2)
FG-V	4	0.16271(1,1)	0.26970(2,1)	0.32685(2,2)	0.35287(3,1)	0.38190(3,2)
	6	0.16270(1,1)	0.26968(1,2)	0.32682(2,2)	0.35284(1,3)	0.38188(3,2)
	8	0.16269(1,1)	0.26967(2,1)	0.32681(2,2)	0.35283(3,1)	0.38187(2,3)
	10	0.16269(1,1)	0.26967(2,1)	0.32681(2,2)	0.35282(1,3)	0.38186(3,2)
	12	0.16269(1,1)	0.26966(2,1)	0.32681(2,2)	0.35282(3,1)	0.38186(3,2)
	14	0.16269(1,1)	0.26966(1,2)	0.32680(2,2)	0.35282(1,3)	0.38186(3,2)

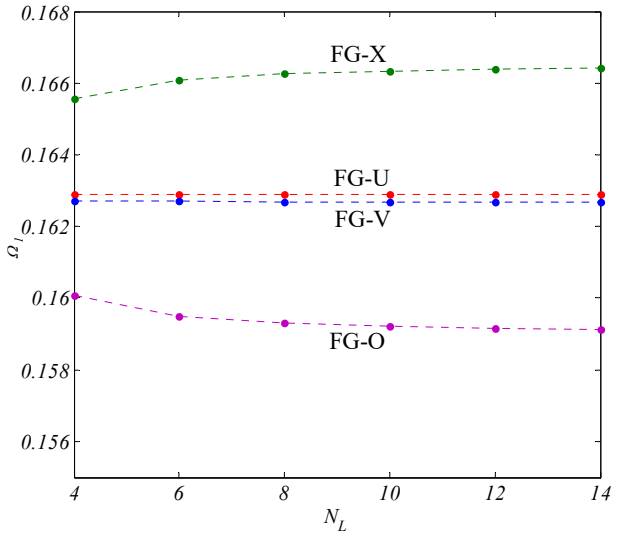

Figure 3. First frequency parameters Ω_1 of an FG-GPLRC square nanoplate for various values of number of layers with $\frac{a}{h} = 5$, $W_{GPL} = 1\%$, and $\lambda = 0.05$.

Another deduction can be stated that, due to the fact that, in X model, GPL-rich layers are located at a greater distance from the middle layer, X-GPLRC nanoplates have greater flexural rigidity and, as a result, higher frequencies [50–54]. On the other hand, in the

O-GPLRC plate, the arrangement of the GPL-rich and GPL-poor layers is the opposite of the X model, as a result of which the lowest flexural rigidity is obtained, and that is why we see the lowest frequencies in association with the O model. Based on the grading function, the two models, V and O, achieve an intermediate level of flexural rigidity compared to the X and O models, and, for this reason, their frequencies are lower than the X model and higher than the O model.

As the second case study, the first six dimensionless frequencies of an FG-GPLRC nanoplate reinforced with 0.5% weight fraction of GPLs distributed based on four types of grading patterns are computed and listed in Table 5 for several values of the non-dimensional nonlocal parameter. In addition, to better obtain the variation in fundamental frequency as a function of nonlocal parameter, Figure 4 is provided. A 10-layer square nanoplate with $a/h = 5$ is considered. One can see clearly that, when the nonlocal parameter is included, the frequencies drop in general. According to Table 5, the growth in dimensionless nonlocal parameter causes a reduction in the frequencies of the nanoplates, and this decrease occurs with the same rate for all four models. It should be noted that the rate of frequency changes with variation in the non-local parameter is greater for frequencies associated with higher modes. As the last tip inferred from Table 5, it should be highlighted that the mode sequence of the frequencies may be affected by variation in the value of the nonlocal parameter. For an example, in X model, with $\lambda = 0.01$, fourth frequency is associated with a vibration mode of (2,2), while, for $\lambda = 0.03$, it belong to a vibration mode of (3,1).

Table 5. First five frequency parameters Ω of an FG-GPLRC square nanoplate for various values of dimensionless nonlocal parameter with $a/h = 5$ and $W_{GPL} = 0.5\%$.

Distribution Pattern	λ	Ω_1	Ω_2	Ω_3	Ω_4	Ω_5
FG-U	0	0.22207(1,1)	0.48611(1,2)	0.56274(1,1)	0.7036(2,2)	0.83186(3,1)
	0.01	0.20294(1,1)	0.39777(2,1)	0.51427(1,1)	0.52596(2,2)	0.59014(3,1)
	0.02	0.18803(1,1)	0.34486(2,1)	0.43812(2,2)	0.47649(1,1)	0.48237(3,1)
	0.03	0.17599(1,1)	0.30865(1,2)	0.38335(2,2)	0.41798(3,1)	0.41798(1,3)
	0.04	0.16600(1,1)	0.28188(1,2)	0.34504(2,2)	0.37397(3,1)	0.37397(1,3)
	0.05	0.15754(1,1)	0.26106(1,2)	0.31631(2,2)	0.34146(3,1)	0.34146(1,3)
FG-X	0	0.22459(1,1)	0.48963(2,1)	0.56278(1,1)	0.70691(2,2)	0.83474(3,1)
	0.01	0.20524(1,1)	0.40066(1,2)	0.51430(1,1)	0.52844(2,2)	0.59218(1,3)
	0.02	0.19017(1,1)	0.34736(2,1)	0.44018(2,2)	0.47652(1,1)	0.48405(3,1)
	0.03	0.17799(1,1)	0.31089(2,1)	0.38515(2,2)	0.41943(1,3)	0.41943(3,1)
	0.04	0.16789(1,1)	0.28393(1,2)	0.34667(2,2)	0.37527(1,3)	0.37527(3,1)
	0.05	0.15933(1,1)	0.26295(1,2)	0.31780(2,2)	0.34265(3,1)	0.34265(1,3)
FG-O	0	0.21944(1,1)	0.48228(2,1)	0.56278(1,1)	0.69979(2,2)	0.82837(3,1)
	0.01	0.20054(1,1)	0.39464(2,1)	0.51430(1,1)	0.52311(2,2)	0.58766(3,1)
	0.02	0.18581(1,1)	0.34214(2,1)	0.43574(2,2)	0.47652(1,1)	0.48035(1,3)
	0.03	0.17391(1,1)	0.30622(2,1)	0.38127(2,2)	0.41622(3,1)	0.41622(1,3)
	0.04	0.16404(1,1)	0.27966(2,1)	0.34317(2,2)	0.37240(3,1)	0.37240(1,3)
	0.05	0.15568(1,1)	0.25900(1,2)	0.31460(2,2)	0.34003(3,1)	0.34003(1,3)
FG-V	0	0.22198(1,1)	0.48596(1,2)	0.56274(1,1)	0.70340(2,2)	0.83164(3,1)
	0.01	0.20286(1,1)	0.39765(1,2)	0.51427(1,1)	0.52581(2,2)	0.58998(3,1)
	0.02	0.18796(1,1)	0.34475(1,2)	0.43799(2,2)	0.47649(1,1)	0.48225(1,3)
	0.03	0.17592(1,1)	0.30856(1,2)	0.38324(2,2)	0.41787(3,1)	0.41787(1,3)
	0.04	0.16594(1,1)	0.28179(2,1)	0.34494(2,2)	0.37388(1,3)	0.37388(3,1)
	0.05	0.15748(1,1)	0.26097(2,1)	0.31622(2,2)	0.34137(1,3)	0.34137(3,1)

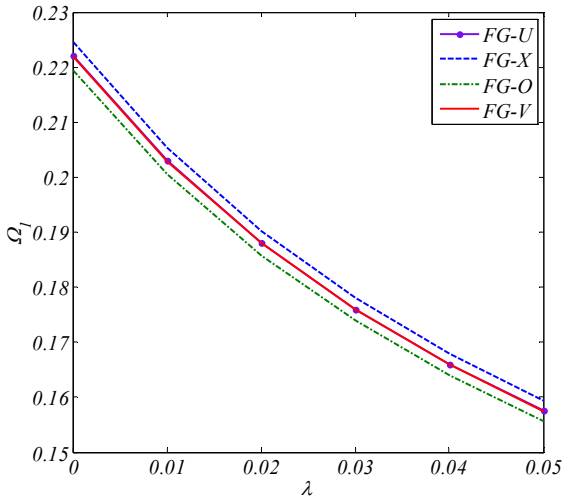

Figure 4. Fundamental frequency parameter Ω_1 of an FG-GPLRC square nanoplate for various values of dimensionless nonlocal parameter with $a/h = 5$ and $W_{GPL} = 0.5\%$.

Next, with the aid of Table 6, the influence of GPL weight fraction on the frequencies of FG-GPLRC nanoplates is investigated. Also, to better extract the variation in fundamental frequency as a function of weight fraction of GPLs, Figure 5 is provided. Numerical results are provided for U-, X-, O-, and V-GPLRC nanoplates with $a/b = 1$ and $a/h = 5$ by applying the non-local dimensionless parameter of 0.05. As can be seen, adding more GPL to the epoxy matrix leads to an increase in the elasticity modulus of each layer, and, as a result, as the extensional, coupled, and flexural stiffness of the structure increase, this results in an increase in frequencies. In fact, when added to composites or other materials, graphene nanoparticles can considerably improve their mechanical characteristics. The materials become stronger and more resilient thanks to their outstanding tensile strength and stiffness [55]. From Table 6, one can see the rate of this increase is faster for X model and slower for O model. Moreover, through the data presented in Table 6, the changes in the sequence of modes can be detected due to the variation in the nonlocal parameter. The fact that graphene may enhance the mechanical properties of reinforced composites is highlighted in many works, such as [54].

Table 6. First six frequency parameters Ω of an FG-GPLRC square nanoplate for various values of GPL weight fraction with $a/h = 5$, $\lambda = 0.05$.

Distribution Pattern	$W_{GPL}\%$	Ω_1	Ω_2	Ω_3	Ω_4	Ω_5
FG-U	0.0	0.15204(1,1)	0.25192(1,2)	0.30523(2,2)	0.32949(3,1)	0.35656(2,3)
	0.2	0.15426(1,1)	0.25560(1,2)	0.30970(2,2)	0.33432(1,3)	0.36178(2,3)
	0.4	0.15645(1,1)	0.25925(2,1)	0.31412(2,2)	0.33909(1,3)	0.36695(2,3)
	0.6	0.15862(1,1)	0.26286(1,2)	0.31850(2,2)	0.34382(3,1)	0.37208(2,3)
	0.8	0.16077(1,1)	0.26643(2,1)	0.32283(2,2)	0.34851(1,3)	0.37715(2,3)
	1.0	0.16290(1,1)	0.26997(1,2)	0.32713(2,2)	0.35315(3,1)	0.38218(3,2)
FG-X	0.0	0.15204(1,1)	0.25192(1,2)	0.30523(2,2)	0.32949(3,1)	0.35656(2,3)
	0.2	0.15499(1,1)	0.25639(2,1)	0.31033(2,2)	0.33483(1,3)	0.36212(2,3)
	0.4	0.15789(1,1)	0.26078(1,2)	0.31533(2,2)	0.34006(1,3)	0.36758(2,3)
	0.6	0.16075(1,1)	0.26510(1,2)	0.32025(2,2)	0.34521(3,1)	0.37294(3,2)
	0.8	0.16357(1,1)	0.26934(1,2)	0.32509(2,2)	0.35027(1,3)	0.37822(3,2)
	1.0	0.16634(1,1)	0.27353(2,1)	0.32986(2,2)	0.35526(1,3)	0.38342(3,2)

Table 6. *Cont.*

Distribution Pattern	W_{GPL}%	Ω_1	Ω_2	Ω_3	Ω_4	Ω_5
FG-O	0.0	0.15204(1,1)	0.25192(1,2)	0.30523(2,2)	0.32949(3,1)	0.35656(2,3)
	0.2	0.15351(1,1)	0.25479(1,2)	0.30903(2,2)	0.33376(3,1)	0.36140(3,2)
	0.4	0.15496(1,1)	0.25761(1,2)	0.31276(2,2)	0.33796(1,3)	0.36615(3,2)
	0.6	0.15639(1,1)	0.26038(2,1)	0.31643(2,2)	0.34208(3,1)	0.37083(3,2)
	0.8	0.15780(1,1)	0.26311(2,1)	0.32004(2,2)	0.34614(1,3)	0.37542(3,2)
	1.0	0.15921(1,1)	0.26581(2,1)	0.32360(2,2)	0.35014(3,1)	0.37995(2,3)
FG-V	0.0	0.15204(1,1)	0.25192(1,2)	0.30523(2,2)	0.32949(3,1)	0.35656(2,3)
	0.2	0.15424(1,1)	0.25559(2,1)	0.30968(2,2)	0.33430(3,1)	0.36177(2,3)
	0.4	0.15641(1,1)	0.25919(1,2)	0.31406(2,2)	0.33903(3,1)	0.36690(3,2)
	0.6	0.15854(1,1)	0.26274(1,2)	0.31837(2,2)	0.34370(3,1)	0.37195(3,2)
	0.8	0.16063(1,1)	0.26623(2,1)	0.32262(2,2)	0.34829(3,1)	0.37694(3,2)
	1.0	0.16269(1,1)	0.26967(2,1)	0.32681(2,2)	0.35282(1,3)	0.38186(2,3)

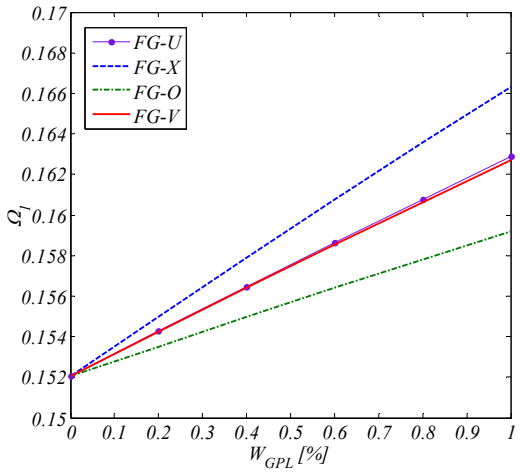

Figure 5. Fundamental frequency parameter Ω_1 of an FG-GPLRC square nanoplate for various values of GPL weight fraction with $a/h = 5, \lambda = 0.05$.

The last parametric study is dedicated to the effect of length-to-thickness ratio on the natural frequencies of functionally graded nanoplates reinforced with 0.5 percent by weight of graphene platelets. The provided data around this study obtained with a dimensionless nonlocal parameter of 0.04 is reported in Table 7. This table demonstrates the length-to-thickness ratio is an effective parameter on the value of frequencies and their mode sequences. Also, it can be highlighted that, for the four reinforcement distribution models, with the increase in the length-to-thickness ratio, the frequencies decrease at almost the same rate.

Table 7. First six frequency parameters Ω of an FG-GPLRC square nanoplate for various values of length-to-thickness ratio with $\lambda = 0.04$ and $W_{GPL} = 0.5\%$.

Distribution Pattern	*a/h*	Ω_1	Ω_2	Ω_3	Ω_4	Ω_5
FG-U	2	0.731410(1,1)	1.051700(1,1)	1.052500(2,1)	1.193100(2,2)	1.289900(2,1)
	5	0.166000(1,1)	0.281880(1,2)	0.345040(2,2)	0.373970(3,1)	0.406340(3,2)
	10	0.045327(1,1)	0.083897(1,2)	0.108900(2,2)	0.121660(1,3)	0.137130(2,3)
	50	0.001874(1,1)	0.003627(1,2)	0.004897(2,2)	0.005604(1,3)	0.006530(2,3)
FG-X	2	0.733050(1,1)	1.050200(2,1)	1.051700(1,1)	1.188800(2,2)	1.290000(2,1)
	5	0.167890(1,1)	0.283930(1,2)	0.346670(2,2)	0.375270(1,3)	0.407170(3,2)
	10	0.045996(1,1)	0.084978(2,1)	0.110140(2,2)	0.122930(1,3)	0.138420(2,3)
	50	0.001905(1,1)	0.003686(2,1)	0.004976(2,2)	0.005693(3,1)	0.006634(3,2)

Table 7. *Cont.*

Distribution Pattern	a/h	Ω_1	Ω_2	Ω_3	Ω_4	Ω_5
FG-O	2	0.729240(1,1)	1.051700(1,1)	1.054100(1,2)	1.196700(2,2)	1.290000(2,1)
	5	0.164040(1,1)	0.279660(2,1)	0.343170(2,2)	0.372400(3,1)	0.405220(3,2)
	10	0.044647(1,1)	0.082784(2,1)	0.107610(2,2)	0.120320(1,3)	0.135770(3,2)
	50	0.001844(1,1)	0.003568(2,1)	0.004818(2,2)	0.005514(1,3)	0.006425(3,2)
FG-V	2	0.731240(1,1)	1.051300(1,1)	1.052300(1,2)	1.193000(2,2)	1.288700(1,2)
	5	0.165940(1,1)	0.281790(2,1)	0.344940(2,2)	0.373880(1,3)	0.406250(2,3)
	10	0.045308(1,1)	0.083864(1,2)	0.108860(2,2)	0.121610(3,1)	0.137090(2,3)
	50	0.001874(1,1)	0.003626(2,1)	0.004895(2,2)	0.005602(1,3)	0.006527(3,2)

9. Conclusions

In the present work, the nonlocal free vibration investigation of functionally graded graphene-platelet-reinforced composite nanoplates has been carried out. By employing a six-variable plate theory that is compatible with the kinematics of arbitrary thick plates, the effects through thickness shear deformations and thickness stretching were taken into account and also the traction free condition on top and bottom surfaces was satisfied. With the accordance of the constraints of the simply supported edges of the nanoplate, a Navier solution method was extended to obtain the inertia and stiffness matrices of the nano-scale structure, and, having them, the frequencies and corresponding mode numbers were calculated. By providing a number of comparison studies, the accuracy of the results was confirmed. After that, parametric studies were planned to evaluate the effects of nonlocal parameters, GPL weight fraction, length-to-thickness ratio, and number of layers on free vibration characteristics. It is concluded that

- with an acceptable accuracy, a ten-layer nanocomposite-laminated nanoplate model can be treated as an FGM plate with continuous variation of material properties.
- By considering the nonlocal elasticity, the frequencies are reduced.
- It was clearly revealed that frequencies are highly affected by non-local parameter changes and this effect is more significant for higher frequencies.
- With the introduction of GPLs in the matrix of the composite nanoplate, frequencies are enhanced.
- FG-X and FG-O patterns have maximum and minimum frequencies of the plate.
- The introduced quasi-3D plate model may serve as an excellent theory for estimation of mechanical response of arbitrary thick plates made of GPLRCs at nano and macro scales.

Author Contributions: Conceptualization, Y.K. and Y.Z.; methodology, Y.K. and Y.Z.; validation, Y.K.; formal analysis, Y.K.; investigation, Y.K. and Y.Z.; writing—original draft preparation, Y.K.; writing—review and editing, Y.K. and Y.Z.; funding acquisition, Y.Z. All authors have read and agreed to the published version of the manuscript.

Funding: This work was supported by the Natural Science Foundation of Inner Mongolia Autonomous Region of China (Grant nos. 2023LHMS05054 and 2023LHMS05017), the Inner Mongolia University of Technology Natural Science Foundation of China (Grant no. DC2200000903), the Program for Innovative Research Teams in Universities of the Inner Mongolia Autonomous Region of China (Grant no. NMGIRT2213), the key technological project of Inner Mongolia (Grant nos. 2021GG0255 and 2021GG0259), and the Fundamental Research Funds for the Directly affiliated Universities of Inner Mongolia Autonomous Region (Grant No. JY20220046).

Data Availability Statement: Data sharing not applicable.

Conflicts of Interest: The authors declare no conflict of interest.

References

1. Rafiee, M.A.; Rafiee, J.; Wang, Z.; Song, H.; Yu, Z.; Koratkar, N. Enhanced Mechanical Properties of Nanocomposites at Low Graphene Content. *ACS Nano* **2009**, *3*, 3884–3890. [CrossRef] [PubMed]
2. Zhao, S.; Zhao, Z.; Yang, Z.; Ke, L.L.; Kitipornchai, S.; Yang, J. Functionally graded graphene reinforced composite structures: A review. *Eng. Struct.* **2020**, *210*, 110339. [CrossRef]
3. Song, M.; Kitipornchai, S.; Yang, J. Free and forced vibrations of functionally graded polymer composite plates reinforced with graphene nanoplatelets. *Compos. Struct.* **2017**, *159*, 579–588. [CrossRef]
4. Guo, H.; Cao, S.; Yang, T.; Chen, Y. Vibration of laminated composite quadrilateral plates reinforced with graphene nanoplatelets using the element-free IMLS-Ritz method. *Int. J. Mech. Sci.* **2018**, *142–143*, 610–621. [CrossRef]
5. Zhao, Z.; Feng, C.; Wang, Y.; Yang, J. Bending and vibration analysis of functionally graded trapezoidal nanocomposite plates reinforced with graphene nanoplatelets (GPLs). *Compos. Struct.* **2017**, *180*, 799–808. [CrossRef]
6. Guo, H.; Cao, S.; Yang, T.; Chen, Y. Geometrically nonlinear analysis of laminated composite quadrilateral plates reinforced with graphene nanoplatelets using the element-free IMLS-Ritz method. *Compos. B Eng.* **2018**, *154*, 216–224. [CrossRef]
7. Gholami, R.; Ansari, R. Nonlinear stability and vibration of pre/post-buckled multilayer FG-GPLRPC rectangular plates. *Appl. Math. Model.* **2019**, *65*, 627–660. [CrossRef]
8. Wu, H.; Yang, J.; Kitipornchai, S. Parametric instability of thermo-mechanically loaded functionally graded graphene reinforced nanocomposite plates. *Int. J. Mech. Sci.* **2018**, *135*, 431–440. [CrossRef]
9. Muni Rami Reddy, R.; Karunasena, W.; Lokuge, W. Free vibration of functionally graded-GPL reinforced composite plates with different boundary conditions. *Aerosp. Sci. Technol.* **2018**, *78*, 147–156. [CrossRef]
10. Gao, K.; Gao, W.; Chen, D.; Yang, J. Nonlinear free vibration of functionally graded graphene platelets reinforced porous nanocomposite plates resting on elastic foundation. *Compos. Struct.* **2018**, *204*, 831–846. [CrossRef]
11. Yang, J.; Chen, D.; Kitipornchai, S. Buckling and free vibration analyses of functionally graded graphene reinforced porous nanocomposite plates based on Chebyshev-Ritz method. *Compos. Struct.* **2018**, *193*, 281–294. [CrossRef]
12. Lin, H.G.; Cao, D.Q.; Xu, Y.Q. Vibration, buckling, aeroelastic analysis of functionally graded multilayer graphene-platelets-reinforced composite plates embedded in piezoelectric layers. *Int. J. Appl. Mech.* **2018**, *10*, 1850023. [CrossRef]
13. Gholami, R.; Ansari, R. On the nonlinear vibrations of polymer nanocomposite rectangular plates reinforced by graphene nanoplatelets: A unified higher-order shear deformable model. *Iran. J. Sci. Technol. Trans. Mech. Eng.* **2019**, *43*, 603–620. [CrossRef]
14. Torabi, J.; Ansari, R. Numerical phase-field vibration analysis of cracked functionally graded GPL-RC plates. *Mech. Based Des. Struct.* **2022**, *50*, 3491–3510. [CrossRef]
15. Pashmforoush, F. Statistical analysis on free vibration behavior of functionally graded nanocomposite plates reinforced by graphene platelets. *Compos. Struct.* **2019**, *213*, 14–24. [CrossRef]
16. Ansari, R.; Hassani, R.; Gholami, R.; Rouhi, H. Free vibration analysis of postbuckled arbitrary-shaped FG-GPL-reinforced porous nanocomposite plates. *Thin Wall. Struct.* **2021**, *163*, 107701. [CrossRef]
17. Zhao, T.Y.; Wang, Y.X.; Pan, H.G.; Gao, X.S.; Cai, Y. Analytical solution for vibration characteristics of rotating graphene nanoplatelet-reinforced plates under rubimpact and thermal shock. *Adv. Compos. Mater.* **2020**, *29*, 1–15.
18. Thai, C.H.; Phung-Van, P. A meshfree approach using naturally stabilized nodal integration for multilayer FG GPLRC complicated plate structures. *Eng. Anal. Bound. Elem.* **2020**, *117*, 346–358. [CrossRef]
19. Jafari, P.; Kiani, Y. Free vibration of functionally graded graphene platelet reinforced plates: A quasi 3D shear and normal deformable plate model. *Compos. Struct.* **2021**, *275*, 114409. [CrossRef]
20. Shi, X.; Suo, R.; Xia, L.; Yu, X.; Babaie, M. Static and free vibration analyses of functionally graded porous skew plates reinforced by graphene platelet based on three-dimensional elasticity theory. *Waves Random Complex Media* **2022**. [CrossRef]
21. Kiani, Y.; Żur, K.K. Free vibrations of graphene platelet reinforced composite skew plates resting on point supports. *Thin Wall. Struct.* **2022**, *176*, 109363. [CrossRef]
22. Abbaspour, F.; Arvin, H.; Shahriari-Kahkeshim, M. Active control of vibrations of piezoelectric rectangular nanocomposite micro plates reinforced with graphene platelet in thermal ambient considering the structural damping. *Int. J. Comp. Methods Eng. Sci. Mech.* **2022**, *23*, 243–262. [CrossRef]
23. Eringen, A.C. Nonlocal polar elastic continua. *Int. J. Eng. Sci.* **1972**, *10*, 1–16. [CrossRef]
24. Thai, C.H.; Nguyen-Xuan, H.; Nguyen-Thanh, N.; Le, T.H.; Nguyen-Thoi, T.; Rabczuk, T. Static, free vibration, and buckling analysis of laminated composite Reissner–Mindlin plates using NURBS-based isogeometric approach. *Int. J. Numer. Methods Eng.* **2012**, *91*, 571–603. [CrossRef]
25. Thai, C.H.; Ferreira, A.J.M.; Bordas, S.P.A.; Rabczuk, T.; Nguyen-Xuan, H. Isogeometric analysis of laminated composite and sandwich plates using a new inverse trigonometric shear deformation theory. *Eur. J. Mech. A* **2014**, *43*, 89–108. [CrossRef]
26. Thai, C.H.; Kulasegaram, S.; Tran, L.V.; Nguyen-Xuan, H. Generalized shear deformation theory for functionally graded isotropic and sandwich plates based on isogeometric approach. *Compos. Struct.* **2014**, *141*, 94–112. [CrossRef]
27. Lu, P.; Zhang, P.Q.; Lee, H.P.; Wang, C.M.; Reddy, J.N. Non-local elastic plate theories. *Proc. R. Soc. A* **2007**, *463*, 3225–3240. [CrossRef]
28. Duan, W.H.; Wang, C.M. Exact solutions for axisymmetric bending of micro/nanoscale circular plates based on nonlocal plate theory. *Nanotechnology* **2007**, *18*, 385704. [CrossRef]

29. Aksencer, T.; Aydogdu, M. Levy type solution method for vibration and buckling of nanoplates using nonlocal elasticity theory. *Phys. E Low Dimens. Syst. Nanostruct.* **2011**, *43*, 954–959. [CrossRef]
30. Pradhan, S.C.; Murmu, T. Small scale effect on the buckling of single-layered graphene sheets under biaxial compression via nonlocal continuum mechanics. *Comput. Mater. Sci.* **2009**, *47*, 268–274. [CrossRef]
31. Pradhan, S.C.; Phadikar, J.K. Small scale effect on vibration of embedded multilayered graphene sheets based on nonlocal continuum models. *Phys. Lett. A* **2009**, *373*, 1062–1069. [CrossRef]
32. Xu, X.; Karami, B.; Janghorban, M. On the dynamics of nanoshells. *Int. J. Eng. Sci.* **2021**, *158*, 103431. [CrossRef]
33. Karami, B.; Janghorban, M.; Tounsi, A. Variational approach for wave dispersion in anisotropic doubly-curved nanoshells based on a new nonlocal strain gradient higher order shell theory. *Thin Wall. Struct.* **2018**, *129*, 251–264. [CrossRef]
34. Karami, B.; Shahsavari, D. On the forced resonant vibration analysis of functionally graded polymer composite doubly-curved nanoshells reinforced with graphene-nanoplatelets. *Comput. Methods Appl. Mech. Eng.* **2020**, *359*, 112767. [CrossRef]
35. Pradhan, S.C.; Phadikar, J.K. Nonlocal elasticity theory for vibration of nanoplates. *J. Sound Vib.* **2009**, *325*, 206–223. [CrossRef]
36. Ansari, R.; Arash, B.; Rouhi, H. Vibration characteristics of embedded multilayered graphene sheets with different boundary conditions via nonlocal elasticity. *Compos. Struct.* **2011**, *93*, 2419–2429. [CrossRef]
37. Ansari, R.; Sahmani, S.; Arash, B. Nonlocal plate model for free vibrations of single-layered graphene sheets. *Phys. Let. A* **2010**, *375*, 53–62. [CrossRef]
38. Panyatong, M.; Chinnaboon, B.; Chucheepsakul, S. Free vibration analysis of FG nanoplates embedded in elastic medium based on second-order shear deformation plate theory and nonlocal elasticity. *Compos. Struct.* **2016**, *153*, 428–441. [CrossRef]
39. Baratim, M.R.; Shahverdim, H. Nonlinear vibration of nonlocal four-variable graded plates with porosities implementing homotopy perturbation and Hamiltonian methods. *Acta Mech.* **2018**, *229*, 343–362. [CrossRef]
40. Aghababaei, R.; Reddy, J.N. Nonlocal third-order shear deformation plate theory with application to bending and vibration of plates. *J. Sound Vib.* **2009**, *326*, 277–289. [CrossRef]
41. Daneshmehr, A.; Rajabpoor, A.; Hadi, A. Size dependent free vibration analysis of nanoplates made of functionally graded materials based on nonlocal elasticity theory with high order theories. *Int. J. Eng. Sci.* **2015**, *95*, 23–35. [CrossRef]
42. Natarajan, S.; Chakraborty, S.; Thangavel, M.; Bordas, S.; Rabczuk, T. Sizedependent free flexural vibration behavior of functionally graded nanoplates. *Comput. Mater. Sci.* **2012**, *65*, 74–80. [CrossRef]
43. Cutolo, A.; Mallardo, V.; Fraldi, M. Third-order nonlocal elasticity in buckling and vibration of functionally graded nanoplates on Winkler-Pasternak media. *Ann. Solid Struct. Mech.* **2020**, *12*, 141–154. [CrossRef]
44. Phung Van, P.; Lieu, X.Q.; Ferreira, A.J.M.; Thai, C.H. A refined nonlocal isogeometric model for multilayer functionally graded graphene platelet-reinforced composite nanoplates. *Compos. Struct.* **2021**, *164*, 107862. [CrossRef]
45. Xie, J.; Li, J.; Zhen, L.; Zhang, C.; Mohammadi, R. A novel nonlocal higher-order theory for the accurate vibration analysis of 2D FG nanoplates. *Proc. Inst. Mech. Eng. Part C* **2022**, *236*, 2161–2171. [CrossRef]
46. Malekzadeh, P.; Shojaee, M. Free vibration of nanoplates based on a nonlocal two-variable refined plate theory. *Compos. Struct.* **2013**, *95*, 443–452. [CrossRef]
47. Sobhy, M.; Radwan, A.F. A New Quasi 3D Nonlocal Plate Theory for Vibration and Buckling of FGM Nanoplates. *Int. J. Appl. Mech.* **2017**, *9*, 1750008. [CrossRef]
48. Kiani, Y.; Mirzaei, M. Isogeometric thermal postbuckling of FG-GPLRC laminated plates. *Steel Comp. Struct.* **2019**, *32*, 821–832.
49. Kiani, Y. NURBS-based thermal buckling analysis of graphene platelet reinforced composite laminated skew plates. *J. Therm. Stress.* **2020**, *43*, 90–108. [CrossRef]
50. Shaoping, B.; Zhang, E.; Babaei, M.; Tornabene, F.; Dimitri, R. The Influence of GPL Reinforcements on the Post-Buckling Behavior of FG Porous Rings Subjected to an External Pressure. *Mathematics* **2023**, *11*, 2421.
51. Ebrahimi, F.; Ezzati, H. A Machine-Learning-Based Model for Buckling Analysis of Thermally Affected Covalently Functionalized Graphene/Epoxy Nanocomposite Beams. *Mathematics* **2023**, *11*, 1496. [CrossRef]
52. Melaibari, A.; Daikh, A.A.; Basha, M.; Abdalla, A.W.; Othman, R.; Almitani, K.H.; Hamed, M.A.; Abdelrahman, A.; Elthaher, M.A. Free Vibration of FG-CNTRCs Nano-Plates/Shells with Temperature-Dependent Properties. *Mathematics* **2022**, *10*, 583. [CrossRef]
53. Melaibari, A.; Daikh, A.A.; Basha, M.; Wagih, A.; Othman, R.; Almitani, K.H.; Hamed, M.A.; Abdelrahman, A.; Elthaher, M.A. A Dynamic Analysis of Randomly Oriented Functionally Graded Carbon Nanotubes/Fiber-Reinforced Composite Laminated Shells with Different Geometries. *Mathematics* **2022**, *10*, 408. [CrossRef]
54. Avey, M.; Fantuzzi, N.; Sofiyev, A. Mathematical Modeling and Analytical Solution of Thermoelastic Stability Problem of Functionally Graded Nanocomposite Cylinders within Different Theories. *Mathematics* **2022**, *10*, 1081. [CrossRef]
55. Animasaun, I.L.; Oke, A.S.; Al-Mdallal, Q.M.; Zidan, A.M. Exploration of water conveying carbon nanotubes, graphene, and copper nanoparticles on impermeable stagnant and moveable walls experiencing variable temperature: Thermal analysis. *J. Therm. Anal. Calorim.* **2023**, *148*, 4513–4522. [CrossRef]